

**Probable causes of the abnormal ridge accompanying the 2013-14 California
drought: ENSO precursor and anthropogenic warming footprint**

S.-Y. Simon Wang,^{1,2} Lawrence Hippias,² Robert R Gillies,^{1,2} and Jin-Ho Yoon³

1. Utah Climate Center, Utah State University, 4825 Old Main Hills, Logan, UT 84322
2. Department of Plants, Soils and Climate, Utah State University, Logan, UT
3. Pacific Northwest National Laboratory, Richland, WA

1. Corresponding author: simon.wang@usu.edu

This article has been accepted for publication and undergone full peer review but has not been through the copyediting, typesetting, pagination and proofreading process which may lead to differences between this version and the Version of Record. Please cite this article as doi: 10.1002/2014GL059748

Abstract

The 2013-14 California drought was accompanied by an anomalous high-amplitude ridge system. The anomalous ridge was investigated using reanalysis data and the Community Earth System Model (CESM). It was found that the ridge emerged from continual sources of Rossby wave energy in the western North Pacific starting in late summer, and subsequently intensified into winter. The ridge generated a surge of wave energy downwind and deepened further the trough over the northeast U.S., forming a dipole. The dipole and associated circulation pattern is not linked directly with either ENSO or Pacific Decadal Oscillation; instead it is correlated with a type of ENSO precursor. The connection between the dipole and ENSO precursor has become stronger since the 1970s, and this is attributed to increased GHG loading as simulated by the CESM. Therefore, there is a traceable anthropogenic warming footprint in the enormous intensity of the anomalous ridge during winter 2013-14, the associated drought and its intensity.

Keywords: California drought; ENSO precursor; Anomalous ridge; Warming effect

1. Introduction

In the winter of 2013-14 California experienced drought conditions that came close to eclipsing the severe drought of 1976-1977 [DWR, 1978]. Periodic drought is endemic to California, even mega droughts between ~900 to 1350 CE [Stine, 1994] and paleo-droughts in the past millennium, have been evident in the past [MacDonald, 2007; Schimmelmann *et al.*, 2003]. Since 38 million people now reside in California, and the state constitutes a major source of food production, the demand for water resources has grown substantially while the impact of droughts keeps growing more profound.

The most immediate cause of the 2013-14 drought conditions was a persistent and high-amplitude upper-level ridge. Figure 1a shows the amplified ridge that was anchored over the Gulf of Alaska from late fall to winter; this prevented synoptic disturbances from reaching and affecting the West Coast. Why did this ‘anomalous’ ridge become both so persistent and so robust? While the winter climate in the West Coast is known to respond to the El Niño-Southern Oscillation (ENSO), and the Pacific Decadal Oscillation (PDO) [Cayan *et al.*, 1999; Dettinger *et al.*, 1998; McCabe and Dettinger, 1999], the winter circulation anomalies did not correspond with either of these oscillations, as ENSO was in a near neutral state and the PDO was not strong in either phase. The lack of connections with ENSO/PDO suggests a deeper question concerning which ocean and atmosphere features might have been at play, i.e., those that could produce such a distinctive ridge pattern as well as the role that climate change might play.

In pursuit of a climate diagnosis of the forcing mechanisms for this drought-producing ridge, we devised two main goals: The first was to quantify the spatial and temporal variability of the atmospheric circulations, and document how these relate to various large-scale climate indices and their associated phases. The second aim was to utilize the fully coupled Community Earth System Model version 1 (CESM1) to see to what extent the model

could simulate the results obtained in the first objective and, to quantify the effects of external forcing factors on the extraordinary amplitude of the ridge.

2. Data Sources

The following datasets were analyzed: the NCEP/NCAR Reanalysis from 1960 to present with a 2.5° lat. x long. resolution [Kalnay *et al.*, 1996]; the Twentieth Century Reanalysis (20CR) from 1871 to 2010 with a 2° resolution [Compo *et al.*, 2011]; the Optimal Interpolation Sea Surface Temperature (OISST) with a 1° resolution [Reynolds *et al.*, 2002], and the NOAA outgoing longwave radiation (OLR) from 1979 with a 2.5° resolution in order to indicate tropical convective activity; NOAA's Precipitation Reconstruction over Land (PREC/L) at 1° resolution [M Chen *et al.*, 2002]. We also analyzed the Historical Single-Forcing Experiments from the CESM1 driven by (a) natural forcing only (NAT, including solar forcing and volcanic aerosols) and (b) greenhouse gas forcing only (GHG), each at 2° resolution. Each CESM1 experiment produced a two-member ensemble initialized from long-stable pre-industrial (year 1850) control settings up to year 2005, as was the case in Wang *et al.* [2013b].

3. The Ridge Formation

The geopotential height anomaly at 250 hPa (Z250) during November 2013-January 2014 (NDJ) is shown in Fig. 1b. It depicts a distinct, east-west circulation “dipole” comprising an abnormal ridge over the Gulf of Alaska and a deepened trough centered north of the Great Lakes. Hereafter this circulation feature will be referred to as “the dipole”. This noteworthy circulation pattern has been linked to some extreme weather events during the winter of 2013-14. While the western ridge is blamed for the widespread drought conditions that have occurred along the West Coast, the eastern trough is associated with the series of

extremely cold outbreaks across the Midwest and East Coast (coined “polar vortex” by NOAA – <http://www.climate.gov/news-features/event-tracker/wobbly-polar-vortex-triggers-extreme-cold-air-outbreak>). The NDJ precipitation deficit is also shown (in terms of the ratio from normal) indicating the extensive dryness that was the case along the West Coast associated with less than 25% of normal precipitation in California.

● Because of these extreme drought and cold events and their apparent link with the dipole, a question was raised regarding the extent to which this circulation pattern was either unique or recurrent as well as its connection to any prominent climate mode(s). Hence, a one-point correlation map of Z250 was constructed based upon the ridge center for the period of 1960-2013. The correlation map in Fig. 1c reveals a pattern broadly similar to that of NDJ 2013-14. The similarity suggests that the dipole is a recurrent feature with a geographical scale beyond western North America. Subsequently, a *dipole index* was constructed by subtracting the Z250 values between the ridge center and the trough center, indicated by the pair of crosses in Fig. 1b. The dipole index values for NDJ since 1960 are shown in Fig. 2a, where it appears that the 2013-14 episode was indeed a record event and in opposite phase to that of 2009-2010. The correlation map of NDJ precipitation over the 1960-2013 period is shown alongside Fig. 1c; this depicts drier conditions associated with the dipole covering the West Coast through central California.

The dipole index and associated circulation pattern was compared to an Empirical Orthogonal Function (EOF) of Z250, shown in Fig. S1. It appears that the dipole index corresponds ($r > 0.6$) to EOF2, while EOF1 and 3 correspond respectively to the PDO and the North Pacific Oscillation (NPO) – a leading pattern of wintertime mid-to-high latitude sea level pressure variability [Linkin and Nigam, 2008; Rogers, 1981]. Through a comparison with various climate indices at NOAA ESRL (<http://www.esrl.noaa.gov/psd/data/climateindices/list/>), we did not find any of the climate

modes that correlate significantly ($p < 0.05$) with either the dipole index or EOF2. However, we did find that the Arctic Oscillation (AO) is moderately correlated ($p < 0.1$) with the dipole index; this will be discussed further in the next section.

The formation process of the western ridge (and the dipole) during NDJ 2013-14 was examined by computing the Rossby wave activity flux, defined by *Takaya and Nakamura* [2001] for the depiction of propagating planetary waves in the mean flows. The anomalies of the 850-hPa geopotential height (Z850) and wave activity fluxes, as well as the OLR, are shown in Fig. 3a for the 3-month averages starting in June-August through NDJ, with a one-month interval. There exists a cross-Pacific pathway of Rossby wave energy, propagating from the western subtropical Pacific towards the Gulf of Alaska; this started in late summer (August-October). The wave activity fluxes intensified during August-October in response to increased convective activity near the Philippine Sea. Downwind of this Rossby wave pathway, over the Gulf of Alaska, a ridge developed during September-November and amplified subsequently in October-December. After October, wave activity over the western North Pacific started to dissipate in association with decreased convective activity in the subtropics. At the upper level (Fig. 3b), wave activity fluxes emanated from Japan from summer through fall. This persistent source of Rossby wave energy arguably contributed to the emergence of the anticyclone over the Gulf of Alaska that persisted and, subsequently, blocked the winter storms from reaching the West Coast. Also noteworthy is the Rossby wave energy dispersed downwind from this ridge, which amplified the trough stationed over northeast North America leading to the so-called “polar vortex”.

4. Link to ENSO Precursor

One striking result of the diagnosis is that the dipole corresponds strongly with circulation features of the year prior to an El Niño, and also appears to be triggered by a wind

and SST pattern that has been identified as a potential long-lead precursor of El Niño. The correlation between the dipole index and the NDJ Niño4 index in the following year (denoted as *Niño4* (*Y+1*)) since 1960 is 0.54, significant at $p < 0.001$. The correlation map of Z250 with Niño4 (*Y+1*) (Fig. 1d) shows prominently the dipole and associated circulation features. The circulation patterns associated with both the dipole and Niño4 (*Y+1*) (Figs. 1c and d) resemble those of the 2013-14 winter (Fig. 1b). Similarity was also present in the precipitation correlations, although the precipitation response to Niño4 (*Y+1*) is considerably weaker than that to the dipole. The broad similarity is also evident in the SST correlation maps shown in Fig. S2, reflecting an ENSO precursor with meridionally stratified SST anomalies across the North Pacific. Such a result suggests that the dipole is indeed linked to a type of ENSO precursor; this will be explained further. Of note, the dipole's correlation with Niño3.4 (*Y+1*) is also significant but at a lower value ($r=0.43$). The reason for the correlation difference between Niño4 and Niño3.4 is unclear, but it may be linked to the observed increase in the occurrence of the El Niño Modoki during the late 20th century [Yeh *et al.*, 2009].

The finding of a recurrent teleconnection one year prior to an ENSO event is critical: Studies focusing on long-lead prediction of ENSO have identified several key patterns across the North Pacific during the preceding winter. Such patterns (i.e. precursors) interact with tropical SST and wind anomalies across the equatorial Pacific and eventually facilitate the development of ENSO in the following year. One such theory is the “Seasonal Footprinting Mechanism” (SFM) from which the NPO imparts a surface wind stress that changes the surface heat fluxes and underlying SST. The SST footprint then lasts into the following summer in the subtropics and potentially impacts equatorial zonal wind stress [Anderson, 2003; Vimont *et al.*, 2001; Vimont *et al.*, 2003]. Under the SFM framework, two precursor patterns are prominent: The Pacific Meridional Mode (PMM) based upon wind and SST

anomalies in the eastern half of the North Pacific [*Chang et al.*, 2007; *Chiang and Vimont*, 2004], and the Western North Pacific (WNP) pattern located in the western part of the basin [*Wang et al.*, 2012; *Wang et al.*, 2013b]. Given the results from Figs. 1d and 3, it is likely that the SST and wind anomalies of the WNP are able to produce a specific teleconnection that contributes to the dipole's formation. Numerous studies [*DeWeaver and Nigam*, 2004; *Jiang and Lau*, 2008; *Lau and Weng*, 2002; *Wang et al.*, 2011] have found that SST and convective activity anomalies in the far western portion of the North Pacific can induce atmospheric short-wave trains that ultimately affect North America in the absence of ENSO. The existence of such wave trains supports the process by which an ENSO precursor can form the dipole through a teleconnection emanating from the WNP.

We were also aware that the AO had reached a strong positive phase in 2013-14 and that it had a moderate correlation of 0.27 with the dipole ($p < 0.1$). In light of this, the indices of AO and Niño4 (Y+1) were plotted as scatters in Fig. 2b. Clearly these two indices are not correlated. However when overlapped with the dipole index and highlighted as those exceeding 2 standard deviations (*cf.* color-filled triangles), two groups stood out. While strong positive phases of the dipole are concentrated in the first quadrant, strong negative phases are clustered in the third quadrant. Here, the Niño4 (Y+1) of NDJ 2013-14 was derived from the January prediction for NDJ 2014-15 (http://www.cpc.ncep.noaa.gov/products/analysis_monitoring/enso_advisory/enso-alert-readme.shtml). Next, a separation boundary of bivariate normal random variables was computed between the 95% confidence level of the probability density of the two groups [*von Storch and Zwiers*, 1999]; this yielded a 15% probability of mis-classification, meaning that only 2 out of 13 significant dipole cases (in either phase) failed to be categorized. The result suggests a modulation by the AO on the dipole, and also echoes the observation by *S Chen et al.* [2013] that the AO may facilitate the development of El Niño a year later via the SFM.

5. Anthropogenic Influence

The record-breaking quality of the extreme drought and the dipole in 2013-14 brings up the role of human influence on climate. For this reason, we examined further whether the dipole has been more active in recent years. Figure 4a shows the running variance of the dipole index over a 30-year window, using the 20CR data. The results reveal an increase in the variance during the 1940-1960 period followed by a decrease in the 1970s, accompanied later by an amplification after 2000; this result was robust regardless of which reanalysis was used. The CESM1 single-forcing simulations were subject to the same variance analysis. It is interesting to note that the CESM1-GHG run simulated a persistent increase in the dipole's variance whereas the CESM1-NAT run produced a decrease after 1970. Such a feature is in concert with recent findings that atmospheric waves in the mid-to-high latitudes have amplified leading to increased extreme events [Screen and Simmonds, 2013; Wang *et al.*, 2013a]. What is more, Figure 4a further suggests that GHG did play a role in the amplification of the dipole.

Since 1960 there has been a growing connection between the WNP pattern and the development of ENSO in the following year [Wang *et al.*, 2013b], which potentially could enhance the dipole – given its link with ENSO precursor. Thus, we examined the sliding correlations between the dipole index and Niño4 (Y+1); this is shown in Fig. 4b. A persistent increase in the 30-year correlations is evident in the observations and becomes significant after the mid-1970s. The CESM1-GHG simulations produced remarkably similar sliding correlations, while the CESM1-NAT run generated insignificant correlations that decreased after 1970. To test the significance for the difference between the two runs, a bootstrapping scheme was applied to 500 pairs of correlated white noise time series that mimicked the distributions of the dipole index and Niño4 (Y+1), following Gershunov *et al.* [2001]. The tests showed that the correlation differences between CESM1-GHG and CESM1-NAT (and

between 20CR and CESM1-NAT) were significant. The correlation maps of simulated Z250 correlated with simulated Niño4 (Y+1) are also shown in Figs. 1e and 1f (and Fig. S2) and they demonstrate good agreement between the dipole and associated circulations among the CESM1 experiments and the observations. The agreement, therefore, lends confidence to the model's ability to capture the dynamical processes inherent within the dipole and ENSO precursor. In terms of modeled precipitation, the simulated dry conditions over California only connected to the ENSO precursor when GHG forcing was introduced. Such a discrepancy requires further research.

6. Summary and Discussion

California's historic drought reached an additional milestone in the winter of 2013-14. Synoptically, an extreme and persistent ridge occupied the Gulf of Alaska for much of the winter; this ridge emerged from persistent sources of Rossby wave energy emanating from the western North Pacific in late summer. The ridge's subsequent intensification generated a surge of wave activity fluxes downwind and deepened the trough over the northeast U.S., forming a dipole. It was found that the dipole and associated large-scale circulation pattern did not correspond directly with any of the prominent climate modes. Instead, it was realized that the dipole was linked with a type of ENSO precursor, namely the WNP pattern. The WNP connection between the dipole and ENSO precursor has strengthened in recent decades. The CESM1 simulations indicated that increased GHG loading in the atmosphere did strengthen the connection between the dipole and ENSO precursor, as well as the dipole's amplitude. It is important to note that the dipole is projected to intensify, which implies that the periodic and inevitable droughts California will experience will exhibit more severity. The inference from this study is that the abnormal intensity of the winter ridge is traceable to human-induced warming but, more importantly, its development is potentially

predictable. Given the increased association with ENSO precursor, the dipole itself could add to our ability to predict North American ENSO. As to the ongoing drought, NOAA's Climate Prediction Center is anticipating an El Niño to develop by summer 2014, with a 50% chance for it to develop into a full-fledged El Niño in the fall. If this El Niño turns out to be strong enough it might provide some drought relief for California due to wet conditions that are consistent with empirical El Niño climatology for the region.

Acknowledgements

Data for this paper are available at NOAA's ESRL and CPC websites. Support came from grants NNX13AC37G and WaterSMART R13AC80039, and the Utah Agricultural Experiment Station.

References

- Anderson, B. T. (2003), Tropical Pacific sea surface temperatures and preceding sea level pressure anomalies in the subtropical North Pacific, *Journal of Geophysical Research*, 108(D23).
- Cayan, D. R., K. T. Redmond, and L. G. Riddle (1999), ENSO and hydrologic extremes in the western United States, *J. Climate*, 12(9).
- Chang, P., L. Zhang, R. Saravanan, D. J. Vimont, J. C. Chiang, L. Ji, H. Seidel, and M. K. Tippett (2007), Pacific meridional mode and El Niño-Southern oscillation, *Geophys. Res. Lett.*, 34(16), L16608.
- Chen, M., P. Xie, J. E. Janowiak, and P. A. Arkin (2002), Global Land Precipitation: A 50-yr Monthly Analysis Based on Gauge Observations, *Journal of Hydrometeorology*, 3(3), 249-266.
- Chen, S., W. Chen, B. Yu, and H.-F. Graf (2013), Modulation of the seasonal footprinting mechanism by the boreal spring Arctic Oscillation, *Geophys. Res. Lett.*, 40(24), 2013GL058628.
- Chiang, J. C. H., and D. J. Vimont (2004), Analogous Pacific and Atlantic Meridional Modes of Tropical Atmosphere-Ocean Variability, *J. Climate*, 17(21), 4143-4158.
- Compo, G. P., J. S. Whitaker, P. D. Sardeshmukh, N. Matsui, R. J. Allan, X. Yin, B. E. Gleason, R. S. Vose, and E. al. (2011), The Twentieth Century Reanalysis Project, *Q. J. Roy. Meteor. Soc.*, 137, 1-28.
- Dettinger, M. D., D. R. Cayan, H. F. Diaz, and D. M. Meko (1998), North-South Precipitation Patterns in Western North America on Interannual-to-Decadal

- Timescales, *J. Climate*, 11(12), 3095-3111.
- DeWeaver, E., and S. Nigam (2004), On the Forcing of ENSO Teleconnections by Anomalous Heating and Cooling, *J. Climate*, 17(16), 3225-3235.
- DWR, C. D. o. W. R.-. (1978), The 1976-1977 California Drought - A Review, edited by D. o. W. Resource, p. 177, California.
- Gershunov, A., N. Schneider, and T. Barnett (2001), Low-frequency modulation of the ENSO–Indian monsoon rainfall relationship: signal or noise?, *J. Climate*, 14(11).
- Jiang, X., and N.-C. Lau (2008), Intraseasonal Teleconnection between North American and Western North Pacific Monsoons with 20-Day Time Scale, *J. Climate*, 21(11), 2664-2679.
- Kalnay, E., et al. (1996), The NCEP/NCAR 40-Year Reanalysis Project, *Bull. Amer. Meteor. Soc.*, 77(3), 437-471.
- Lau, K.-M., and H. Weng (2002), Recurrent Teleconnection Patterns Linking Summertime Precipitation Variability over East Asia and North America, *Journal of the Meteorological Society of Japan*, 80(6), 1309-1324.
- Linkin, M. E., and S. Nigam (2008), The north pacific oscillation-west Pacific teleconnection pattern: Mature-phase structure and winter impacts, *J. Climate*, 21(9), 1979-1997.
- Ludescher, J., A. Gozolchiani, M. I. Bogachev, A. Bunde, S. Havlin, and H. J. Schellnhuber (2014), Very early warning of next El Niño, *Proc. Natl. Acad. Sci.*, 111(6), 2064-2066.
- MacDonald, G. M. (2007), Severe and sustained drought in southern California and the West: Present conditions and insights from the past on causes and impacts, *Quaternary International*, 173, 87-100.
- McCabe, G. J., and M. D. Dettinger (1999), Decadal variations in the strength of ENSO teleconnections with precipitation in the western United States, *Inter. J. Climatol.*, 19(13), 1399-1410.
- Reynolds, R. W., N. A. Rayner, T. M. Smith, D. C. Stokes, and W. Wang (2002), An Improved In Situ and Satellite SST Analysis for Climate, *J. Climate*, 15(13), 1609-1625.
- Rogers, J. C. (1981), The North Pacific Oscillation, *Journal of Climatology*, 1(1), 39-57.
- Schimmelmann, A., C. B. Lange, and B. J. Meggers (2003), Palaeoclimatic and archaeological evidence for a 200-yr recurrence of floods and droughts linking California, Mesoamerica and South America over the past 2000 years, *The Holocene*, 13(5), 763-778.
- Screen, J. A., and I. Simmonds (2013), Exploring links between Arctic amplification and mid-latitude weather, *Geophys. Res. Lett.*, n/a-n/a.
- Stine, S. (1994), Extreme and persistent drought in California and Patagonia during mediaeval time, *Nature*, 369(6481), 546-549.
- Takaya, K., and H. Nakamura (2001), A Formulation of a Phase-Independent Wave-Activity Flux for Stationary and Migratory Quasigeostrophic Eddies on a Zonally Varying Basic Flow, *J. Atmos. Sci.*, 58(6), 608-627.
- Vimont, D. J., D. S. Battisti, and A. C. Hirst (2001), Footprinting: A seasonal connection between the tropics and mid-latitudes, *Geophys. Res. Lett.*, 28(20), 3923-3926.

Vimont, D. J., J. M. Wallace, and D. S. Battisti (2003), The Seasonal Footprinting Mechanism in the Pacific: Implications for ENSO, *J. Climate*, 16(16), 2668-2675.

von Storch, H., and F. W. Zwiers (1999), *Statistical Analysis in Climate Research (Ch.6)*, Cambridge University Press.

Wang, S.-Y., M. L'Heureux, and H.-H. Chia (2012), ENSO prediction one year in advance using western North Pacific sea surface temperatures, *Geophys. Res. Lett.*, 39(5), L05702.

Wang, S.-Y., R. E. Davies, and R. R. Gillies (2013a), Identification of extreme precipitation threat across midlatitude regions based on short-wave circulations, *Journal of Geophysical Research: Atmospheres*, 118(19), 2013JD020153.

Wang, S.-Y., M. L'Heureux, and J.-H. Yoon (2013b), Are greenhouse gases changing ENSO precursors in the Western North Pacific?, *J. Climate*, 26, 6409-6322.

Wang, S.-Y., R. R. Gillies, L. E. Hipps, and J. Jin (2011), A transition-phase teleconnection of the Pacific quasi-decadal oscillation, *Clim. Dynamics*, 36, 681-693.

Yeh, S.-W., J.-S. Kug, B. Dewitte, M.-H. Kwon, B. P. Kirtman, and F.-F. Jin (2009), El Nino in a changing climate, *Nature*, 461(7263), 511-514.

Accepted Article

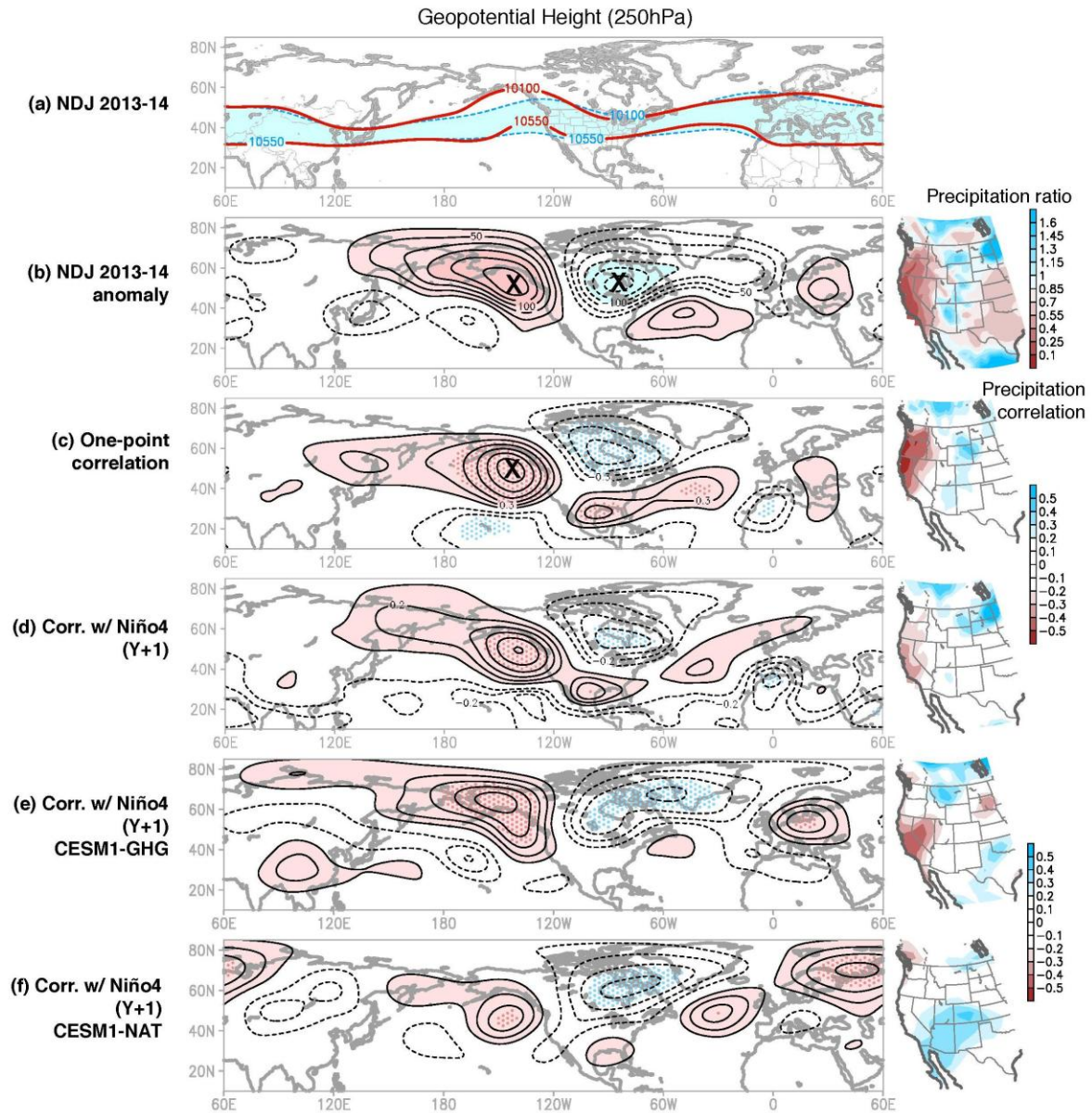


Fig. 1 (a) NDJ 250-hPa geopotential height (Z250) contours of 10100 and 10550 m for the climatology (blue dashed) and during 2013-14 (red solid). (b) The departure of NDJ Z250 from the climatology. (c) One-point correlation of Z250 with the ridge center (cross) for the period 1960-2013; contour interval is 0.15 omitting zero. (d) Correlation map of Z250 correlated with Niño4 (Y+1). (e) and (f) are the same as (d) but from the CESM1-GHG and CESM1-NAT runs. Significant correlations at $p < 0.05$ are dotted. The corresponding correlation maps of NDJ precipitation are shown in the right.

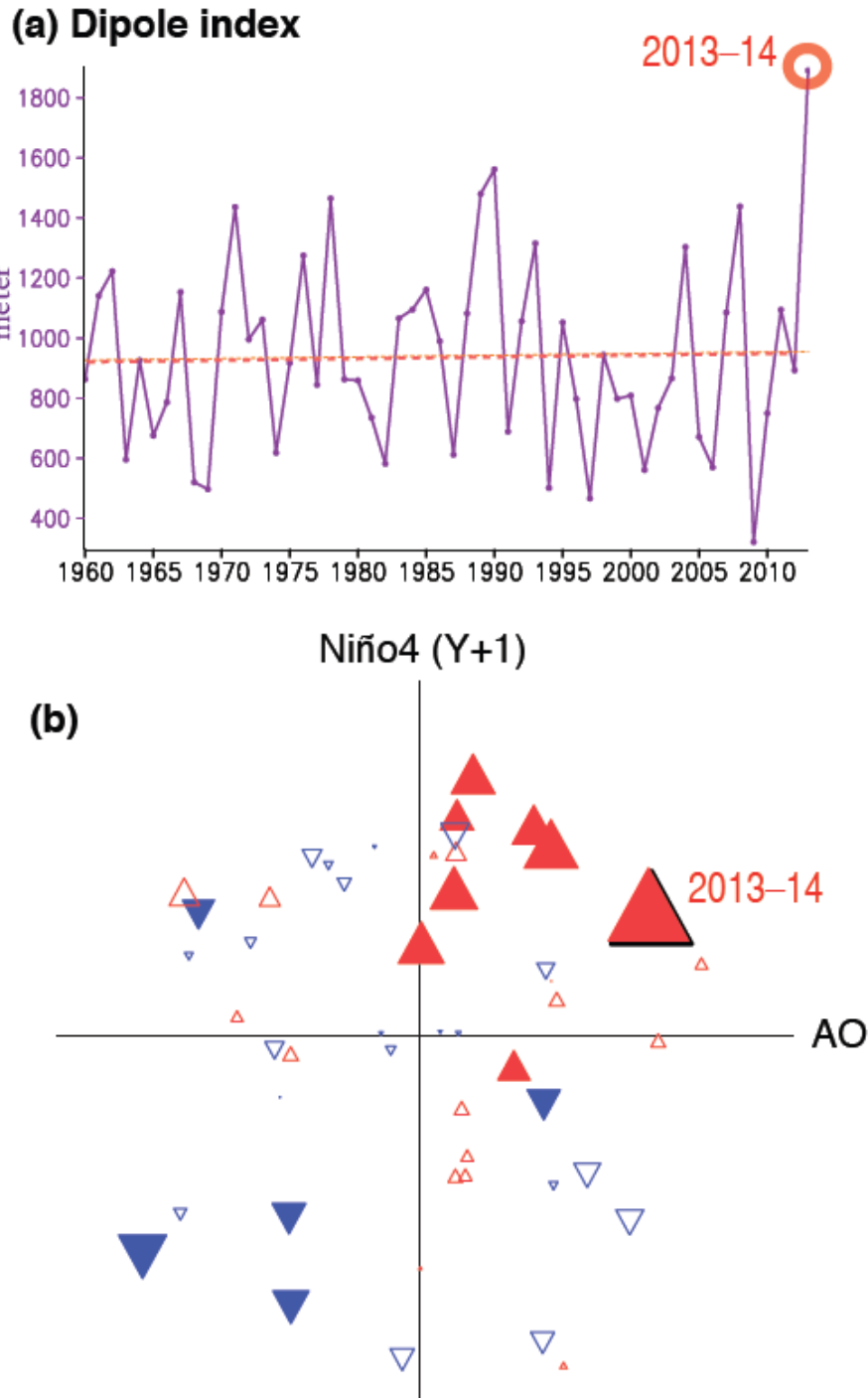


Fig. 2 (a) Time series of the dipole index (NDJ season) based upon the NCEP Reanalysis overlaid with the linear trend (dashed line, not significant). (b) Scatter plot for the AO and Niño4 (Y+1) indices for 1960-2013 with the scatters represented by values of the dipole index; all three indices are standardized (between -1 and 1). Red/blue triangles indicate positive/negative values, while those exceeding 2 standard deviations are color-filled.

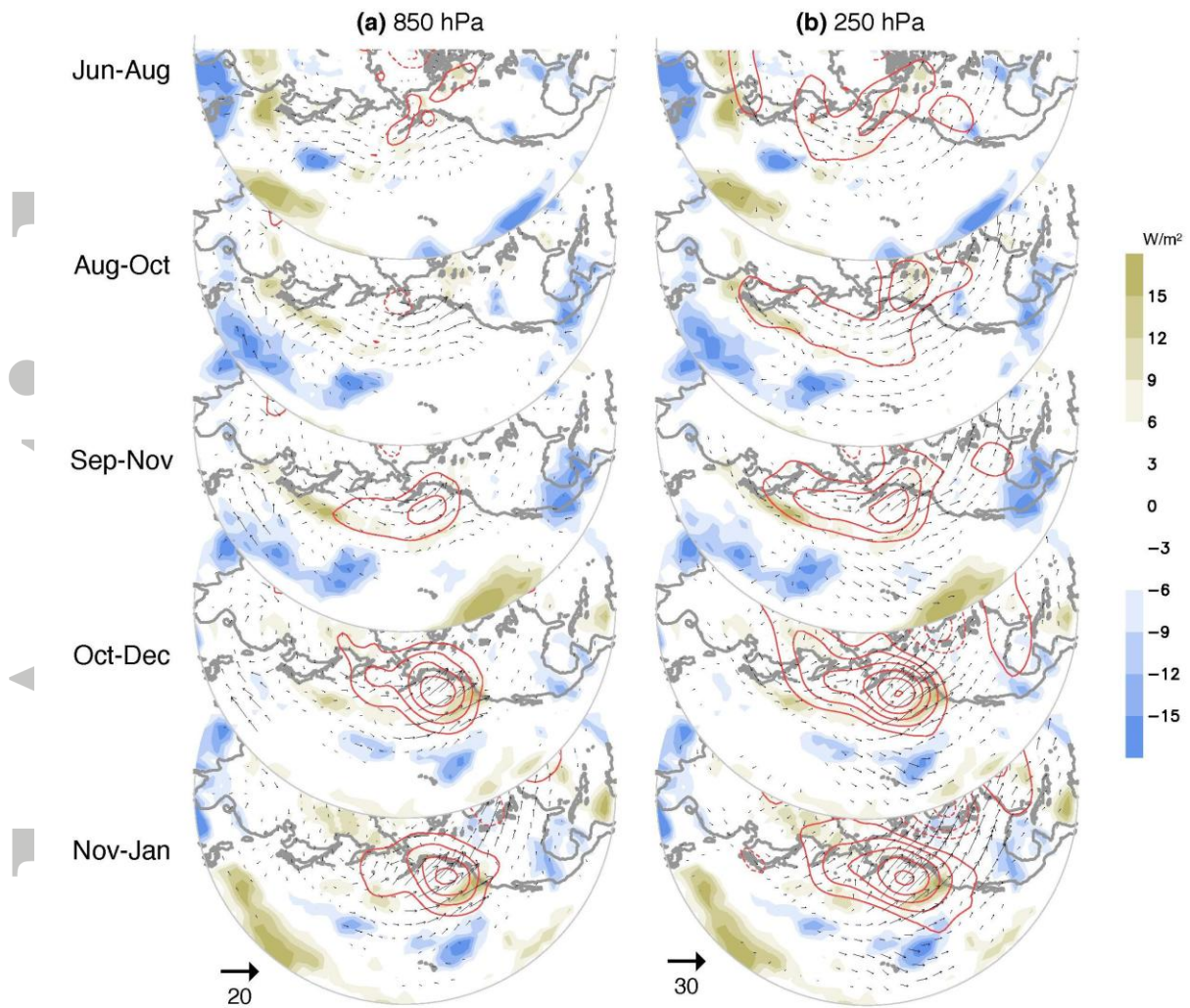


Fig. 3 NDJ 2013-14 anomalies of geopotential height (red contours) and OLR (color shadings) overlaid with the wave activity fluxes (vectors, $m^2 s^{-2}$) for a three-month period from June-August to NDJ as indicated, computed from the levels of (a) 850 hPa and (b) 250 hPa. Contour interval is 25 m for 850 hPa and 50 m for 250 hPa; the zero and the first positive and negative contours are omitted.

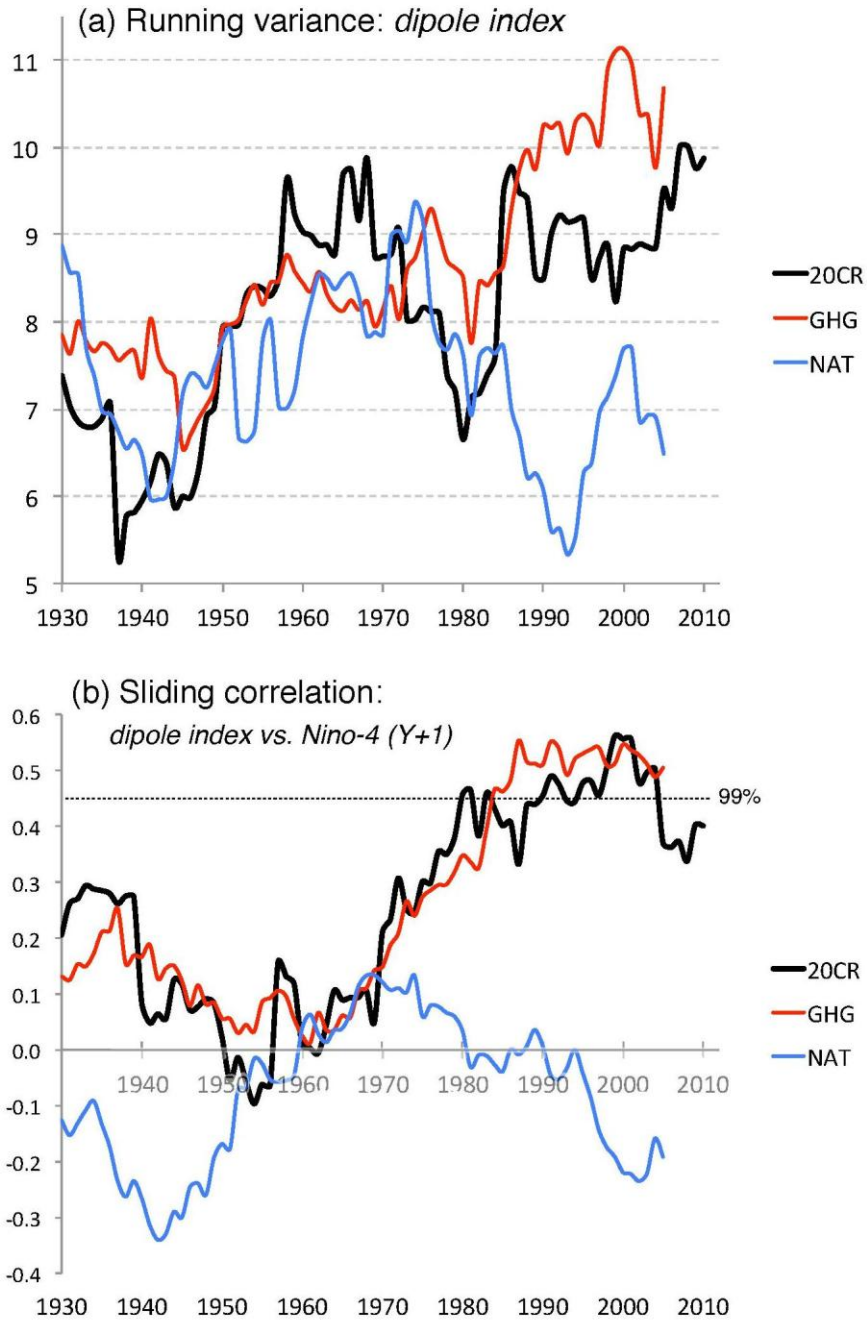


Fig. 4 (a) Running variance of the dipole index ($\times 10^4 \text{ m}^2$) with a 30-year window plotted at the end year beginning in 1900, derived from the 20CR (black), CESM1-GHG run (red) and CESM1-NAT run (blue). (b) Sliding correlations between the dipole index and Niño4 (Y+1) within a 30-year window corresponding to (a). The dashed line indicates significance at the 99% level.